








Cite this: *Soft Matter*, 2017, 13, 6189

Stretching of surface-tethered polymers in pressure-driven flow under confinement†

Tamal Roy, ^a Kai Szuttor, ^b Jens Smiatek, ^b Christian Holm ^b and Steffen Hardt ^{*a}

We study the effect of pressure-driven flow on a single surface-tethered DNA molecule confined between parallel surfaces. The influence of flow and channel parameters as well as the length of the molecules on their extension and orientation is explored. In the experiments the chain conformations are imaged by laser scanning confocal microscopy. We find that the fractional extension of the tethered DNA molecules mainly depends on the wall shear stress, with effects of confinement being very weak. Experiments performed with molecules of different contour length show that the fractional extension is a universal function of the product of the wall shear stress and the contour length, a result that can be obtained from a simple scaling relation. The experimental results are in good agreement with results from coarse-grained molecular dynamics/Lattice-Boltzmann simulations.

Received 13th February 2017,
Accepted 20th July 2017

DOI: 10.1039/c7sm00306d

rsc.li/soft-matter-journal

1 Introduction

The behavior of end-grafted polymers on a surface is in the focus of a number of recent research activities. It is related to practical applications in such fields as colloid or biological science, ranging from steric stabilization of colloidal suspensions^{1,2} to DNA micro array technology.^{3,4} Recent developments in microfluidic technologies have facilitated the observation and manipulation of anchored polymer chains in micro- or nanochannels.^{5–8} Corresponding studies are useful for getting insight into a number of practically relevant scenarios such as the enhancement of sliding between surfaces,^{2,9,10} sequencing of DNA molecules by Genome Sequence Scanning (GSS) or Direct Linear Analysis (DLA)¹¹ and lubrication in articular joints¹⁰ using polymer brushes. Knowledge of the conformation of an end-tethered polymer exposed to a hydrodynamic flow under confinement is therefore necessary for understanding such systems.

Long-chain polymers behave differently in micro or nano-confinement as compared to an unconfined environment. Furthermore, the dynamics of such polymers near a solid interface is still not completely understood. Microfluidic devices have been extensively used to determine the physical properties of polyelectrolytes.^{12–14} Manipulation of polyelectrolytes in a microfluidic environment uses different techniques such as deposition on a substrate (using a receding fluid meniscus¹⁵ or

an evaporating droplet¹⁶), a flow field¹⁷ or an electric field.^{18–21} However, a surface deposition technique may involve an unwanted surface-mediated effect on the dynamics of the molecules. A flow-based technique, instead, becomes advantageous in respect of minimizing the surface-mediated effects and capturing the dynamics of the molecules at the same time. The behavior of a tethered polymer in uniform and shear flow has been studied both experimentally^{22–31} and numerically.^{32–36} DNA molecules are extensively used as a model polymer in corresponding experiments due to their physiological relevance, well-documented properties, versatility as building block for macromolecular structures, and excellent chemical modifiability. Perkins *et al.*²² showed experimentally that for a tethered DNA molecule in uniform flow the fractional extension, which is the ratio of the observed extension x of the molecule in flow direction and its contour length L , only depends on the combination $uL^{0.54}$, where u is the flow velocity. The exponent of L clearly indicates the presence of intrachain hydrodynamic interactions in the stretching dynamics of the DNA molecules. Ladoux *et al.*²³ showed that for a DNA molecule tethered to a surface in the strong stretching limit, the fractional extension scales as $(1 - \dot{\gamma}^{-1/3})$, where $\dot{\gamma}$ is the characteristic shear rate. In this limit, intrachain hydrodynamic interactions are negligible.³⁷ Bakajin *et al.*²⁶ studied the electrohydrodynamic stretching and relaxation of DNA molecules inside a slit-like confinement and reported that the extension of the molecules increases with decreasing slit height. An experimental study of the stretching dynamics of a surface-tethered DNA molecule confined in a microchannel of height smaller than the contour length of the molecule and exposed to a pressure-driven flow, to the best of our knowledge, was not conducted so far.

^a Institute for Nano- and Microfluidics, Technische Universität Darmstadt, Darmstadt, Germany. E-mail: hardt@nmf.tu-darmstadt.de; Fax: +49-6151-16-24278; Tel: +49-6151-16-24274

^b Institut für Computerphysik, Universität Stuttgart, Stuttgart, Germany

† Electronic supplementary information (ESI) available. See DOI: 10.1039/c7sm00306d

In this work, we study a surface-tethered DNA molecule in pressure-driven flow inside microchannels of very small aspect ratio. The height of the channels was chosen smaller than the chain length of the DNA molecules. Such a system not only reduces the required flow rate and amount of flow buffer to control the conformations of the tethered molecules, but facilitates the visualization and detection methods also. In most of the experimental set ups, single DNA molecules are visualized by a high magnification and high numerical aperture objective. A typical value of working distance for such an objective is about 200 μm . It is therefore advantageous to use shallow channels to be able to cover the entire height of the channels and study the tethered molecules (and thus countering the uncertainties of chemical tethering of the DNA molecules). The experimental results are compared to numerical simulations and analyzed based on simple scaling relations.

2 Experimental details

2.1 Materials

SU-8 was purchased from Microchem, PDMS from Dow Corning (Sylgard 184 Silicone elastomer kit). λ -DNA and YOYO-1 were purchased from Invitrogen. The dNTP set, biotin-dUTP, and Klenow exo^- are from Thermo Scientific. Streptavidin, β -mercaptoethanol and (3-glycidyloxypropyl) trimethoxysilane (GPTMS) were purchased from Sigma-Aldrich.

2.2 Microchannel fabrication

SU-8 structures were fabricated using UV lithography. A mixture of PDMS and cross-linker (10:1) was poured onto the structured wafer and heated to 80 $^{\circ}\text{C}$ for 1 hour to obtain a negative of the SU-8 master. That way, channel structures of different height (3.6, 6, 6.7, 7.6 and 70 μm) and width (40–80 μm) and a length of 10 mm were obtained. After punching inlet and outlet holes, the channels were covered with 170 μm thick glass coverslips by oxygen plasma activation.

2.3 Surface modification of microchannels

Tethering of λ -DNA to the channel surface was realized using the well-known biotin–streptavidin affinity. The channel surface containing hydroxyl groups after oxygen plasma activation was treated with a solution of GPTMS (1% v/v) in 95% ethanol for 5 minutes to enhance streptavidin adsorption.^{38,39} After rinsing off the GPTMS, the channels were filled with 0.01 mg mL^{-1} aqueous streptavidin solution and kept at 4 $^{\circ}\text{C}$ overnight for streptavidin adsorption. After that, the channels were rinsed with water to remove the streptavidin.

2.4 DNA sample preparation

The concatenation of the λ -DNA molecules was done using the complementary single-stranded overhangs at the ends of the molecules. 1 μL of 0.33 $\mu\text{g mL}^{-1}$ λ -DNA, 4 μL of 5 \times T4 DNA ligase buffer, 1 μL of T4 DNA ligase (1 U μL^{-1}) and autoclaved water (total volume of 20 μL) were filled into an Eppendorf tube. After mixing thoroughly, the reagents were subsequently

kept at room temperature for 25 minutes. Finally, the concatenated DNA molecules were separated from the reagents by ethanol precipitation.

One end of the λ -DNA or the concatenated λ -DNA was selectively modified with biotin, taking advantage of the single-stranded overhangs at the end of the molecules. The base sequence of one of the overhangs is (ds-DNA)-TCCAGCGGCGGG-5'. The DNA molecules were exposed to a mixture of dATP, dGTP, and biotin-dUTP in the presence of the Klenow exo^- enzyme to produce λ -DNA with only one end of the molecule modified with biotin. The reaction was carried out at 37 $^{\circ}\text{C}$ (ThermoMixer) for 20 minutes, followed by addition of excess EDTA to stop the reaction. The biotinylated DNA sample was separated from unreacted nucleotides by ethanol precipitation. The obtained concentrated sample was diluted with 0.5 \times TE (10 mmol Tris, 1 mmol EDTA, 10 mmol NaCl, pH \approx 8.0) buffer to a concentration of \approx 0.1 $\mu\text{g mL}^{-1}$. Subsequently, the DNA molecules were dyed with the YOYO-1 intercalating dye (staining ratio 1:5). The dyed sample was further diluted with 0.5 \times TE to obtain a final concentration of \approx 100 pg mL^{-1} . Then, the sample was introduced into the streptavidin-functionalized microchannels and left there for 10 minutes for tethering. Finally, the inlet and outlet reservoirs were emptied and subsequently filled with buffer solution (TE, 2% β -mercaptoethanol to prevent photobleaching) which is the medium flowing through the channels.

2.5 Fluorescence microscopy

The experimental set up is shown in Fig. 1. Visualization of single DNA molecules was performed by fluorescence microscopy with a Nikon Eclipse Ti-E inverted laser scanning confocal microscope using a 100 \times oil-immersion objective (NA 1.4). An argon laser (488 nm) was used to excite the intercalating dye, and the emitted signal (at 509 nm) was captured by an Andor CCD camera with 100 ms exposure time. The dynamics of the DNA molecules was recorded in 2D (*i.e.* focusing on a single plane to observe the tethered molecule) by epifluorescence microscopy. Conformations of

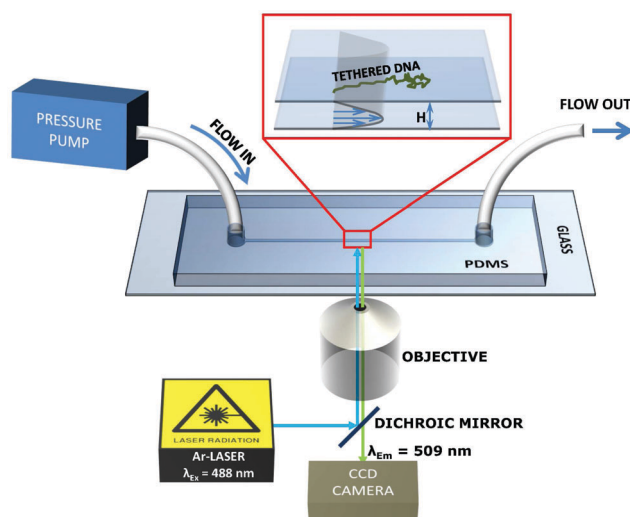


Fig. 1 Schematic diagram of the experimental setup.

the molecule were imaged in 3D by confocal microscopy. Recording of 2D movies and processing of 3D confocal microscopy images was done using the NIS Elements software. Recording of confocal 3D image-stacks was done with the EZ-C1 software. 2D movies were split into images by the FreeStudio software, and the image analysis was done by MATLAB scripts.

2.6 Flow control

The channel with the DNA sample was connected to a pressure pump (Elveflow) containing the buffer solution. The pressure pump was controlled by a MATLAB graphical user interface. The pressure for each channel height was chosen in such a way that the tethered molecule experiences a sufficiently high flow rate (*i.e.* when the extension of the molecule remains almost constant with further increase in the flow rate) or shear stress. Subsequently, the flow rate was reduced in steps of 5 s duration. This duration is significantly larger than the smallest relaxation time of λ -DNA. Therefore, it is expected that the molecules attain a steady-state conformation during each step.

3 Simulation details

The coarse-grained molecular dynamics/Lattice-Boltzmann simulations were performed with the software package ESPResSo.^{40,41} A simple bead-spring model represents the polymer with a purely repulsive shifted and truncated Lennard-Jones potential (Weeks–Chandler–Andersen potential⁴²) according to

$$U_{\text{WCA}}(r) = \begin{cases} 4\varepsilon \left[\left(\frac{b}{r}\right)^{12} - \left(\frac{b}{r}\right)^6 \right] + \varepsilon, & \text{if } r < 2^{1/6}b \\ 0, & \text{else,} \end{cases} \quad (1)$$

where b is the diameter of the bead, r the distance between interacting beads and $\varepsilon = 1k_{\text{B}}T$ the energetic prefactor with the Boltzmann constant k_{B} and temperature T . Adjacent beads are connected by a finitely extensible nonlinear elastic (FENE) bond potential

$$U_{\text{FENE}}(r) = -\frac{1}{2}K\Delta r_{\text{max}}^2 \ln \left[1 - \left(\frac{r}{\Delta r_{\text{max}}}\right)^2 \right], \quad (2)$$

with the spring constant $K = 30\varepsilon/b^2$ and the maximum elongation $\Delta r_{\text{max}} = 1.5b$. The mass of a single bead is $m = 1m_0$. The number of beads is represented by N such that a full extension of the chain scales with $L \sim N$. Furthermore, a mass density of $\rho = 1m_0/b^3$ and a kinematic viscosity of $\nu_{\text{K}} = 1b^2/t$ with the time scale $t = b\sqrt{m_0/\varepsilon}$ are used for the fluid properties. In order to include hydrodynamic interactions, the beads are coupled to a thermalized Lattice-Boltzmann (LB) fluid.^{43,44} The details of the simulation method are described in the ESI.[†]

4 Results and discussion

The fluorescent dye, intercalating with the DNA molecules, untwists the double-helix and as a result, the contour length of the dyed molecule increases. However, this increase in

contour length is a statistical process depending on the number of intercalating dye molecules. Therefore, the chain length of dyed DNA molecules is not known *a priori* but needs to be determined. The extension of a tethered DNA molecule reaches an asymptotic value at very high flow velocities where, for given dynamic viscosity of the flow buffer, the fractional extension of the molecule scales as $\left(1 - \dot{\gamma}_{\text{wall}}^{-1/3}\right)$, where $\dot{\gamma}_{\text{wall}}$ is the wall shear rate.²³ In this extension regime, the fractional extension is only a weak function of contour length of the molecule. We therefore determine the contour length L by a linear fit of x vs. $\dot{\gamma}_{\text{wall}}^{-1/3}$, using four consecutive data points in the highest shear stress regime. To obtain a non-dimensional quantity, the measured extension is normalized by L . We compared our method to an alternative method of determining the contour length. In the alternative method the contour length is obtained from the staining ratio.¹⁹ According to the staining ratio used in our experiments (1 dye molecule per 5 base pairs), the estimated contour length is 20.4 μm . The plot showing the comparison is included in the ESI.[†] (Fig. S2) and indicates the validity of using the scaling relation to determine the contour length.

4.1 Effect of channel height and flow rate

To explore the effect of confinement on the conformation of a tethered DNA molecule, we applied a maximum flow rate of 0.5 $\mu\text{L h}^{-1}$ for $H = 3.6 \mu\text{m}$, of 1.5 $\mu\text{L h}^{-1}$ for $H = 6 \mu\text{m}$, of 1.6 $\mu\text{L h}^{-1}$ for $H = 6.7 \mu\text{m}$, of 3 $\mu\text{L h}^{-1}$ for $H = 7.6 \mu\text{m}$, and of 100 $\mu\text{L h}^{-1}$ for $H = 70 \mu\text{m}$. To study molecules of approximately the same contour length, extensions of 20 μm to 22 μm long λ -DNA molecules were recorded at different flow rates. For each channel height, extensions of at least 7 different molecules were studied. A molecule stretches as a result of the shear stresses caused by the flow. Since during this process the polymer chain remains quite close to the wall it is tethered to (to be discussed below), we identify the wall shear stress τ_{wall} as the parameter determining the steady-state configurations. The shear stress can be varied either by varying the channel height at constant flow rate or by varying the flow rate at constant channel height. To relate the shear stress to the applied pressure, we employ the analytical expression for the laminar flow profile in channels of rectangular cross section,⁴⁵ *i.e.*

$$\tau_{\text{wall}} = \frac{4H\Delta p}{\pi^2 l} \sum_{n,\text{odd}} \frac{1}{n^2} \left[1 - \frac{\cosh \frac{n\pi y}{H}}{\cosh \frac{n\pi W}{2H}} \right], \quad (3)$$

where H , W and l are the height, width and length of the channel respectively, Δp is the pressure difference applied across the channel, and y is the lateral position of the tethering point of the DNA molecule on the channel surface, measured from the centerline of the channel.

The resulting fractional extension of the DNA molecules as a function of wall shear stress is shown in Fig. 2a. The figure contains data obtained with different channel heights. L is the average contour length of at least 7 different DNA molecules (with standard deviation σ). The wall shear stress depends on the position of the tethering point (along the direction normal

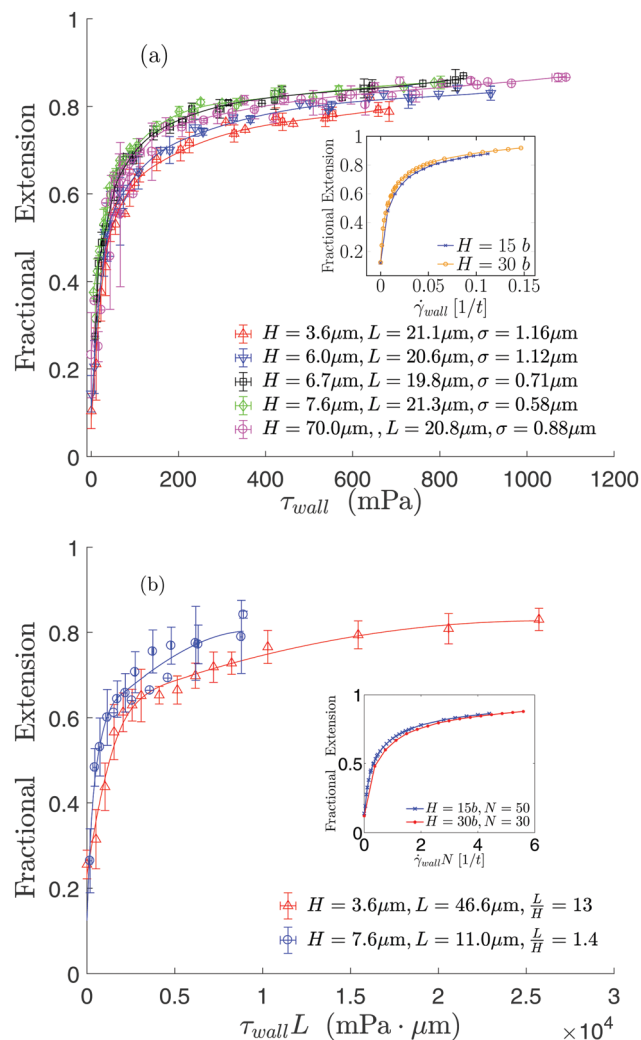


Fig. 2 (a) Extension characteristics of λ -DNA tethered inside channels of different heights. The symbols depict the experimentally determined extension as a function of the wall shear stress. The lines represent B-spline fits to the experimental data. (b) Extension characteristics of concatenated or partially broken λ -DNA tethered inside channels of different heights. The symbols depict the experimentally determined extension as a function of the product of the wall shear stress and the contour length. The lines represent B-spline fits to the experimental data. The two insets show corresponding results of coarse-grained molecular dynamics/Lattice-Boltzmann simulations, where the shear rate takes the role of shear stress. The values of the contour length are $50b$ in part (a) and $30b$ as well as $50b$ in part (b), with the monomer diameter b .

to the flow on the tethering plane). Since the position of the tethering point is not easy to control, we incorporated data binning on the wall shear stress with a bin range of 30 mPa and included error bars in wall shear stress (represented by the standard deviation of the values of wall shear stress within the bin range). The error bars in fractional extension represent the standard deviation of the set of fractional extension values which correspond to the wall shear stress within the bin range of 5 mPa for $\tau_{\text{wall}} \leq 100$ mPa and 30 mPa for $\tau_{\text{wall}} > 100$ mPa. Due to the uncertainty in the position of the tethering points, some data points on the Fig. 2 do not contain any error bar.

When the fractional extension is plotted as a function of the wall shear stress, within the experimental error bars the data sets obtained with different channels collapse to a single curve, except for slight deviations of the data obtained in the $H = 3.6$ and $6 \mu\text{m}$ channels. This deviation could possibly be attributed to the exposure of the fluctuating chain (normal to the flow direction) to the non-linear velocity profile at a distance from the wall.

A useful parameter which represents the degree of confinement can be defined by the ratio of the molecular contour length and the channel height (*i.e.* $\frac{L}{H}$). An increase of this ratio indicates an increasing confinement. For the experimental data shown in Fig. 2a, the range of this ratio is $2.7 \lesssim \frac{L}{H} \lesssim 5.7$. To study a wider range of confinement and to understand the influence of the velocity profile away from the tethering plane on the stretching of the molecules, we conducted similar experiments with concatenated λ -DNA molecules in a $3.6 \mu\text{m}$ deep channel and partially broken λ -DNA in a $7.6 \mu\text{m}$ deep channel. These two cases (apart from the $70 \mu\text{m}$ deep channel) represent the extremes with the highest and lowest degree of confinement ($1.4 \lesssim \frac{L}{H} \lesssim 13$). Fig. 2b shows the corresponding variation of the fractional extension with the wall shear stress. The hydrodynamic drag force (responsible for the stretching) increases with the size of a molecule. Therefore, to eliminate the size-dependency, we plotted the fractional extension as a function of the product of the wall shear stress and the contour length (see Section 4.2). We note that the extension characteristics for these two extreme degrees of confinement is almost the same (with a slight reduction of the fractional extension in the shallower channel). A quantitative analysis of the difference in the extension curves corresponding to these extreme cases is presented in Section S5 of the ESI.† The analysis indicates a weak influence of confinement. Upon an increase of the confinement by a factor of 9.2, a maximum decrease of the fractional extension by about 10% is obtained. Therefore, the effect of confinement is very weak, and the wall shear stress appears to be the predominant factor controlling the extension of the molecules.

To uncover the reason for this dependence of the molecular extension exclusively on the wall shear stress, we imaged the molecular conformations at different shear stresses using laser scanning confocal microscopy. The three dimensional images of the DNA molecules, represented by two different views (top view onto the tethering plane and side view along the tethering plane and perpendicular to the flow direction) are shown in Fig. 3 for different values of the wall shear stress. The details of the confocal microscopy image processing are given in Section S6 of the ESI.† In these projected views we notice that under a small wall shear stress (*e.g.* $\tau_{\text{wall}} < 50$ mPa), a molecule is weakly stretched and the part it is exposed to the velocity profile away from the tethering plane. When a molecule stretches significantly, it always remains close to the wall, *i.e.* it does not significantly penetrate into the central region of the channel. It is therefore possible to identify two different stretching regimes of a chain described as the weak-stretching and the strong-stretching regime.

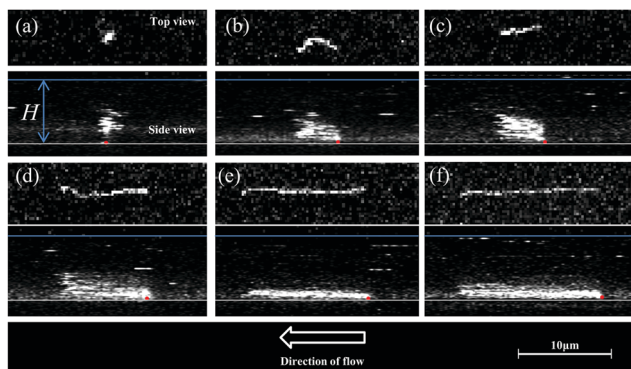


Fig. 3 3D confocal microscopy images of surface-tethered λ -DNA inside a 6.7 μm high and 50 μm wide channel at different wall shear stresses (a) 0 mPa, (b) 4.9 mPa, (c) 24.5 mPa, (d) 49 mPa, (e) 245.2 mPa, (f) 490.3 mPa. The extension in (f) is 15.7 μm . The contour length is 19.1 μm . The tethering point is indicated by the red dot in each side view.

To study the stretching of tethered molecules in these two regimes and to identify the range of the wall shear stress where the transition between these two regimes takes place, we conducted similar experiments with concatenated λ -DNA molecules. The tethered concatenated molecules were exposed to a low shear rate to ensure that they were able to sample as much as possible of the velocity profile away from the tethering plane. In Fig. 4 we plot the fractional extension of the concatenated λ -DNA molecules against the wall shear stress. At low enough values of the wall shear stress the fractional extension can be expressed as $x/L \sim \tau_{\text{wall}}^m$. A linear fit of the corresponding data points indicates $m \sim 0.50$. The value of the scaling exponent m for λ -DNA molecules obtained with different channel heights is shown in Fig. S3 of ESI† and varies between 0.37 and 0.60. The range of the scaling exponent indicates that in this regime,

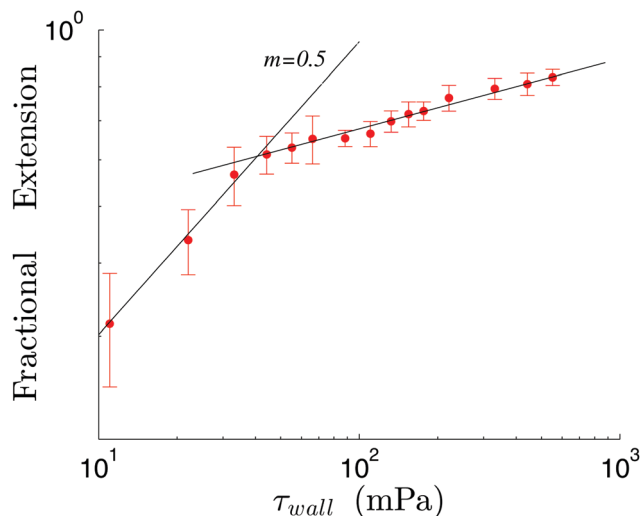


Fig. 4 Fractional extension of concatenated λ -DNA ($L = 46.6 \mu\text{m}$, $\sigma = 2 \mu\text{m}$) in 3.6 μm deep channels. The fractional extension data in weak and strong stretching regimes are fitted to two different straight lines. The line indicated by the slope $m = 0.5$ represents a fit to the data in weak stretching regime.

the stretching of the chain can be described by the stem-and-flower model proposed by Brochard-Wyart,⁴⁶ where $x \sim \tau_{\text{wall}}^{\frac{1}{2}}$. The two different slopes of the data shown in Fig. 4 indicate the wall shear stress corresponding to the onset of strong stretching. For the considered molecules with a contour length of about 47 μm and also for λ -DNA molecules with a contour length of $\sim 21 \mu\text{m}$ (as indicated in Fig. S3 of ESI†), this value is about 50 mPa. The molecules are, therefore, strongly stretched and remain very close to the tethering surface over a wide range of the applied wall shear stress, which is the predominant factor responsible for stretching.

The overall picture indicates that the stretching of surface-tethered DNA molecules is governed exclusively by the shear stress at the wall to which the molecule is attached, with only a very weak influence of the confinement (*i.e.* the relative size of the molecule compared to the channel height). The inset plots in Fig. 2 show the results of molecular dynamics simulations performed for similar systems as in our experiments. Like the experiments, the simulation results also indicate that the fractional extension is uniquely determined by the wall shear rate (or the wall shear stress, if the viscosity of the fluid is kept constant) and that the influence of confinement is very weak. To compare the results obtained with confined DNA molecules to those obtained without confinement ($H > L$), we also performed the same experiment in 70 μm high channels. The result shows that the fractional extension depends in a similar way on the wall shear stress as in the confined environment (*cf.* Fig. 2).

The angle of orientation (α) of the chain with the tethering surface is shown as a function of the wall shear stress for different channel heights in Fig. 5. We notice that already at a very small value of wall shear stress ($\sim 50 \text{ mPa}$), the angle of orientation approaches a value of 10° , which indicates that the chain is almost parallel to the surface and remains very close to the surface. This explains that the quantity determining the

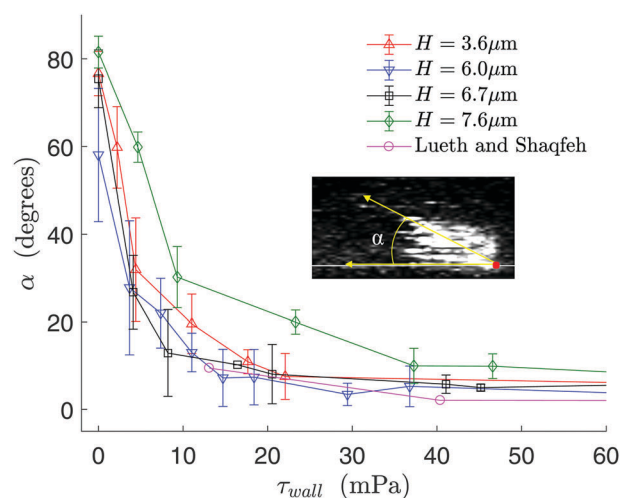


Fig. 5 Angle of orientation of surface-tethered λ -DNA plotted against the wall shear stress for different channel heights. The average contour length of the molecules is $\sim 20 \mu\text{m}$. The lines are guides to the eye.

stretching of the molecules is the wall shear stress rather than a complex functional accounting also for the shear stresses inside the channel. In Fig. 5, we compare the polymer orientation in our experiments with the polymer orientation in the experiments carried out by Lueth and Shaqfeh.³¹ Lueth and Shaqfeh used laser etched 100 μm deep fused quartz coverslips pressed against a PDMS backing and tethered the DNA molecules on the inner surface of the etched quartz cell. A pressure-driven Poiseuille flow was then applied on the tethered molecules. On a length scale of the radius of gyration of the tethered molecule, the flow was effectively a linear shear flow near the tethering plane. This setup resembles our experimental setup except for the channel height used. We notice that the plot of the orientation angle with wall shear stress for λ -DNA from the experiments of Lueth and Shaqfeh is similar to the corresponding plot from our experiments. These results indicate agreement with our statement that the channel height only has a weak influence on the stretching and orientation of the tethered chains in the strong-stretching regime (*i.e.* $\tau_{\text{wall}} \gtrsim 50$ mPa). The variation of the orientation angle over a larger range of wall shear stress (0–600 mPa) is shown in Fig. S4 of ESI.†

4.2 Effect of chain length of the DNA molecules

The surface-tethered DNA molecules are extended by pressure-driven flow. The measured steady-state extensions of the chains are, therefore, solely results of the balance of hydrodynamic drag (which extends the chain) and the entropic recoiling force (or the entropic spring force, which pulls the chain back to its random coil conformation). Fig. 2 and 5 indicate that the tethered chain assumes a stretched conformation even at a small value of τ_{wall} . Here we develop a scaling relationship between the extension of the chains, the wall shear stress, and the chain length.

The chain can be represented by N small segments connected in series. The length of each segment is equal to the persistence length of the polymer. The hydrodynamic drag force exerted by the Poiseuille flow on each segment is expressed as

$$f_d = \zeta \int_0^H P(y)u(y)dy \quad (4)$$

where ζ is the drag coefficient of each segment, $P(y)$ is the probability of finding the segment at a distance y from the tethering plane and $u(y)$ is the flow velocity. The probability distribution $P(y)$ will definitely be different for the segments near the tethering point. However, for long chains, most of the segments are likely to have the same probability distribution and therefore, using the same probability distribution for each segment will not introduce much error. For simplicity, we assume the flow to be a plane Poiseuille flow with a velocity profile

$$u(y) = \frac{\tau_{\text{wall}}}{\eta H}(Hy - y^2) \quad (5)$$

where η is the dynamic viscosity. The average distance between the chain and the wall can be expressed as

$$\Delta y \sim \int_0^H yP(y)dy \quad (6)$$

The exact form of f_d depends on the functional form of $P(y)$. However, in an order-of-magnitude sense, we can write

$$\int_0^H y^2 P(y)dy \sim (\Delta y)^2 \quad (7)$$

The intrachain hydrodynamic interaction is screened due to the presence of the solid surface^{26,47} and the strongly stretched conformation^{37,48} (even at a small value of the wall shear stress, see Fig. 2). Furthermore, a comparison of the stretching behavior with and without intrachain hydrodynamic interactions was made possible by comparing the results from coarse grained MD/LB simulations and Langevin dynamics simulations on a confined surface-tethered polymer.⁴⁹ The comparison indicates that the hydrodynamic interactions can be safely ignored in the strong-stretching regime. Therefore, the effective drag coefficient of the entire chain is directly proportional to the chain length L . The hydrodynamic drag force on the entire chain is expressed as

$$F_d \sim \frac{\zeta \tau_{\text{wall}} L \Delta y}{\eta b} \left(1 - \frac{\Delta y}{H}\right). \quad (8)$$

Eqn (8) represents a generic expression of the stretching force (of hydrodynamic origin) on a surface-tethered chain, and the ratio $\frac{\Delta y}{H}$ appearing on the r.h.s. represents the relative magnitude of the transverse fluctuation (in the direction normal to the tethering surface) of the chain. A larger value of this ratio indicates that the chain is exposed to the non-linear velocity profile away from the surface and therefore, in a shallower channel we expect a slight reduction of hydrodynamic drag force. From our experimental results we conclude that the moderate confinement does not play a significant role in the stretching of the tethered chains. Only a slight reduction of the fractional extension with increasing degree of confinement is observed (as shown in Fig. 2). Confocal microscopy images (Fig. 3) and Fig. 4 show that the chains are stretched and very close to the tethering surface over a wide range of the wall shear stress (> 50 mPa). Therefore, the ratio $\Delta y/H$ is small compared to 1 for the range of H values considered here. With this, to a good approximation eqn (8) reduces to

$$F_d \sim \frac{\zeta \tau_{\text{wall}} L \Delta y}{\eta b}. \quad (9)$$

Confocal microscopy images (Fig. 3) show that the variation of Δy with τ_{wall} is negligible for a stretched chain.

On the other hand, the entropic recoiling force acting on the chain can be expressed as a function of the fractional extension.^{50,51} *i.e.*

$$F_s = g\left(\frac{x}{L}\right), \quad (10)$$

The functional form of g depends on the appropriate model to describe the chain dynamics. In steady state $F_d = F_s$, which results in

$$\frac{x}{L} \sim h(\tau_{\text{wall}} L). \quad (11)$$

The functional form of h depends on the forms of g and ζ .

We performed the experiment with different sizes of tethered DNA molecules confined in 7.6 μm high microchannels. For that purpose, we used partially broken (by the flow) and concatenated tethered λ -DNA molecules to obtain a variation in the contour length. The corresponding values of the contour length are 11 μm , 17.4 μm , 21.6 μm , 26.4 μm and 36.5 μm . Each value of the contour length is the average of the contour lengths of at least 5 different DNA molecules (with standard deviation σ , as indicated in Fig. 6). To analyze the experimental data, we plot the fractional extension as a function of $\tau_{\text{wall}} L$ (Fig. 6). The error bars in the fractional extension and $\tau_{\text{wall}} L$ are included due to the uncertainty in the position of the tethering point as explained in Section 4.1. The plot shows that the data points for DNA molecules of different contour length collapse to form a universal curve within the error bars. The statistical significance of this statement is discussed in Section S5 of the ESI.† Clearly, the intention of such an analysis is not to completely rule out the effects of confinement, which are to a certain degree visible in Fig. 2b. However, the range of the confinement covered in the experiments corresponding to Fig. 6 is $1.4 \lesssim \frac{L}{H} \lesssim 4.8$, where, according to our analysis, the effects of confinement can be neglected. The inset plot in Fig. 6 shows coarse-grained molecular dynamics/Lattice-Boltzmann simulation

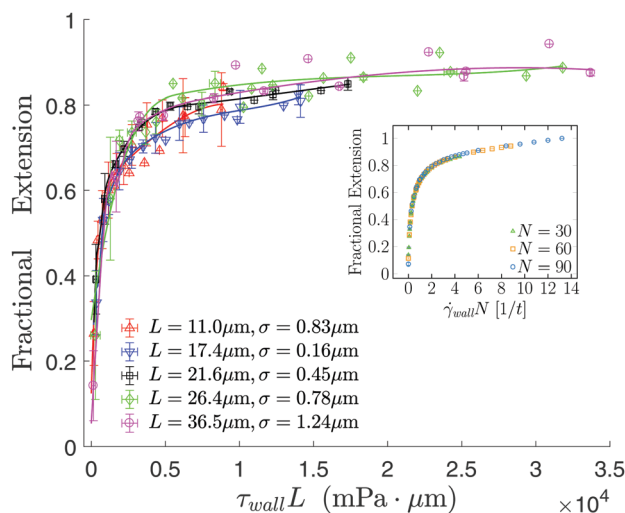


Fig. 6 Master curve of fractional extension plotted against the similarity variable. The main diagram depicts the experimentally determined extension as a function of the product of the wall shear stress and the respective molecular contour length. The lines represent B-spline fits to the experimental data. The inset shows the result the coarse-grained molecular dynamics/Lattice-Boltzmann simulations, where the fractional extension is plotted as a function of the product of the wall shear rate and the respective number of monomers. The channel height considered in the simulation was 30b.

results for confined end-tethered chains of different lengths (characterized by the number of monomer N) in pressure-driven flow. Similar to the experimental results, the fractional extension of the chains shows a universal functional relationship with $\dot{\gamma}_{\text{wall}} N$. This is in agreement with our model derived from simple scaling arguments (eqn (11)).

5 Conclusions

We experimentally investigated the stretching of surface-tethered long DNA molecules exposed to pressure-driven flow inside a microchannel of height smaller than the contour length of the molecules. The experiments were based on imaging single molecules stained with a fluorescent dye. We found that the fractional extension of a tethered chain is a function of the shear stress at the wall surface to which the molecule is tethered. In the weak-stretching regime, the fractional extension of a chain follows the scaling of stem-and-flower model proposed by Brochard-Wyart.⁴⁶ In the strong-stretching regime, the fractional extension is a function of the wall shear stress and the chain length. In this regime, there is only a very weak influence of the degree of confinement, which can be explained by the fact that over a wide range of the wall shear stress the chain always remains close to the surface. We also explored the effect of the chain length on the fractional extension and derived a scaling model for the dependence of the extension on the wall shear stress and the chain length in the strong-stretching regime. The fractional extension is a universal function of the product of the wall shear stress and contour length of the molecule. The experimental results are consistent with the assumption that intrachain hydrodynamic interactions are screened due to the proximity of the stretched chains to the tethering plane. Both the scaling relationship and the weak dependence of the stretching on the channel height are in agreement with results obtained from coarse-grained molecular dynamics/Lattice-Boltzmann simulations.

Acknowledgements

We are grateful to Farough Roustaei, Institut für Elektromechanische Konstruktionen, Technische Universität Darmstadt, for the preparation of SU-8 master structures. Financial assistance of the Deutsche Forschungsgemeinschaft (grant no. HA 2696/33-1 and HO 1108/22-1) is gratefully acknowledged.

References

- 1 H. Dautzenberg, *Acta Polym.*, 1985, **36**, 457.
- 2 M. Lyons, I. Prigogine and S. Rice, *Advances in Chemical Physics, Polymeric Systems*, 1997.
- 3 C. E. Gagna and W. C. Lambert, *Pharmacogenomics*, 2009, **10**, 895–914.
- 4 A. N. Rao and D. W. Grainger, *Biomater. Sci.*, 2014, **2**, 436–471.
- 5 D. J. Mai, C. Brockman and C. M. Schroeder, *Soft Matter*, 2012, **8**, 10560–10572.

- 6 S. L. Levy and H. G. Craighead, *Chem. Soc. Rev.*, 2010, **39**, 1133–1152.
- 7 K. T. Sørensen, J. M. Lopacinska, N. Tommerup, A. Silahatoglu, A. Kristensen and R. Marie, *Rev. Sci. Instrum.*, 2015, **86**, 063702.
- 8 S. M. Friedrich, H. C. Zec and T.-H. Wang, *Lab Chip*, 2016, **16**, 790–811.
- 9 J. F. Joanny, *Langmuir*, 1992, **8**, 989–995.
- 10 S. Milner, *Science*, 1991, **251**, 905–914.
- 11 E. Y. Chan, N. M. Goncalves, R. A. Haeusler, A. J. Hatch, J. W. Larson, A. M. Maletta, G. R. Yantz, E. D. Carstea, M. Fuchs and G. G. Wong, *et al.*, *Genome Res.*, 2004, **14**, 1137–1146.
- 12 R. Bazoni, C. Lima, E. Ramos and M. Rocha, *Soft Matter*, 2015, **11**, 4306–4314.
- 13 F. Latinwo and C. M. Schroeder, *Soft Matter*, 2014, **10**, 2178–2187.
- 14 T. Strick, J.-F. Allemand, V. Croquette and D. Bensimon, *Prog. Biophys. Mol. Biol.*, 2000, **74**, 115–140.
- 15 X. Michalet, R. Ekong, F. Fougerousse, S. Rousseaux, C. Schurra, N. Hornigold, M. Van Slegtenhorst, J. Wolfe, S. Povey and J. S. Beckmann, *et al.*, *Science*, 1997, **277**, 1518–1523.
- 16 W. Wang, J. Lin and D. C. Schwartz, *Biophys. J.*, 1998, **75**, 513–520.
- 17 E. S. Shaqfeh, *J. Non-Newtonian Fluid Mech.*, 2005, **130**, 1–28.
- 18 G. C. Randall, K. M. Schultz and P. S. Doyle, *Lab Chip*, 2006, **6**, 516–525.
- 19 S. Ferree and H. W. Blanch, *Biophys. J.*, 2003, **85**, 2539–2546.
- 20 T. Hahn and S. Hardt, *Soft Matter*, 2011, **7**, 6320–6326.
- 21 T. Hahn and S. Hardt, *Anal. Chem.*, 2011, **83**, 5476–5479.
- 22 T. T. Perkins, D. E. Smith, R. G. Larson and S. Chu, *Science*, 1995, **268**, 83.
- 23 B. Ladoux and P. Doyle, *Europhys. Lett.*, 2000, **52**, 511.
- 24 P. S. Doyle, B. Ladoux and J.-L. Viovy, *Phys. Rev. Lett.*, 2000, **84**, 4769.
- 25 J. Wang and C. Lu, *J. Appl. Phys.*, 2007, **102**, 074703.
- 26 O. Bakajin, T. Duke, C. Chou, S. Chan, R. Austin and E. Cox, *Phys. Rev. Lett.*, 1998, **80**, 2737.
- 27 K. Jo, Y.-L. Chen, J. J. de Pablo and D. C. Schwartz, *Lab Chip*, 2009, **9**, 2348–2355.
- 28 J. W. Larson, G. R. Yantz, Q. Zhong, R. Charnas, C. M. D'Antoni, M. V. Gallo, K. A. Gillis, L. A. Neely, K. M. Phillips and G. G. Wong, *et al.*, *Lab Chip*, 2006, **6**, 1187–1199.
- 29 C. B. Renner and P. S. Doyle, *Soft Matter*, 2015, **11**, 3105–3114.
- 30 S. Gerashchenko and V. Steinberg, *Phys. Rev. Lett.*, 2006, **96**, 038304.
- 31 C. A. Lueth and E. S. Shaqfeh, *Macromolecules*, 2009, **42**, 9170–9182.
- 32 R. Rzehak, W. Kromen, T. Kawakatsu and W. Zimmermann, *Eur. Phys. J. E: Soft Matter Biol. Phys.*, 2000, **2**, 3–30.
- 33 D. Stigter and C. Bustamante, *Biophys. J.*, 1998, **75**, 1197–1210.
- 34 C. E. Sing and A. Alexander-Katz, *Macromolecules*, 2011, **44**, 9020–9028.
- 35 Y. Gratton and G. Slater, *Eur. Phys. J. E: Soft Matter Biol. Phys.*, 2005, **17**, 455–465.
- 36 R. M. Jendrejack, E. T. Dimalanta, D. C. Schwartz, M. D. Graham and J. J. de Pablo, *Phys. Rev. Lett.*, 2003, **91**, 038102.
- 37 J. W. Hatfield and S. R. Quake, *Phys. Rev. Lett.*, 1999, **82**, 3548.
- 38 C. Mateo, V. Grazu, J. M. Palomo, F. Lopez-Gallego, R. Fernandez-Lafuente and J. M. Guisan, *Nat. Protoc.*, 2007, **2**, 1022–1033.
- 39 Q. Zhang, R. Huang and L.-H. Guo, *Chin. Sci. Bull.*, 2009, **54**, 2620–2626.
- 40 H. J. Limbach, A. Arnold, B. A. Mann and C. Holm, *Comput. Phys. Commun.*, 2006, **174**, 704–727.
- 41 A. Arnold, O. Lenz, S. Kesselheim, R. Weeber, F. Fahrenberger, D. Roehm, P. Košovan and C. Holm, *Meshfree Methods for Partial Differential Equations VI*, Springer, 2013, pp. 1–23.
- 42 J. D. Weeks, D. Chandler and H. C. Andersen, *J. Chem. Phys.*, 1971, **54**, 5237.
- 43 B. Dünweg and A. J. Ladd, *Lattice Boltzmann Simulations of Soft Matter Systems*, Springer, 2008.
- 44 D. Röhm and A. Arnold, *Eur. Phys. J.: Spec. Top.*, 2012, **210**, 89–100.
- 45 H. Bruus, *Theoretical Microfluidics*, Oxford University Press, New York, 2008.
- 46 F. Brochard-Wyart, *Europhys. Lett.*, 1993, **23**, 105.
- 47 F. Brochard and P. De Gennes, *J. Chem. Phys.*, 1977, **67**, 52–56.
- 48 R. Larson, T. Perkins, D. Smith and S. Chu, *Phys. Rev. E: Stat. Phys., Plasmas, Fluids, Relat. Interdiscip. Top.*, 1997, **55**, 1794.
- 49 K. Szuttor, T. Roy, S. Hardt, C. Holm and J. Smiatek, *J. Chem. Phys.*, 2017, **147**, 034902.
- 50 J. F. Marko and E. D. Siggia, *Macromolecules*, 1995, **28**, 8759–8770.
- 51 S. B. Smith, L. Finzi and C. Bustamante, *Science*, 1992, **258**, 1122–1126.